NUCLEAR REACTIONS -- THEORY

COEXISTENCE OF REGULAR UNDAMPED NUCLEAR DYNAMICS WITH INTRINSIC CHAOTICITY

David A. McGrew, Wolfgang Bauer, Vladimir Zelevinsky[a], and Peter Schuck [b]

The origin of dissipation from collective motion in finite Fermi systems such as atomic nuclei [1] is not completely understood. The mutual balance of one-body and two-body processes is still a question of debate. To understand the interaction between a collective multipole moment and the individual nucleons, Blocki *et al.* [2] consider a classical gas of particles contained in a deformed container undergoing periodic deformations. The deformations are multipole dependent and oscillate with frequencies much smaller than typical single particle frequencies. For octupole and higher deformations the kinetic energy of the particles increases and the particles move chaotically. However, this model is not consistent in that it has a 'collective coordinate' (the deformation of the wall) that is independent from, rather than a sum of, the single particle coordinates.

We introduce selfconsistency into the problem of motion in multipole-deformed nuclear potentials. We use the Bohr-Mottelson [3] type of interaction with a static potential of the form r^2 or r^6 and a quadrupole or octupole interaction through which the nucleons can exchange energy, as studied by Stringari *et al.* [4.5.6] We also investigate the case with static r^2 or r^6 potentials and static quadrupole or octupole moments, which are similar to the Bohr-Mottleson model but do not allow the exchange of energy between nucleons. These cases provide comparison with the Bohr-Mottelson cases.

We treat these problems in a semi-classical approximation by a Wigner transform of the von Neumann equation of motion for the density matrix, $i\partial_t \rho = [\mathcal{H}, \rho]$, to obtain a Vlasov equation $\partial_t f = \{\mathcal{H}, f\}$. We then solve the Vlasov equation in the test particle method [7,8] using a fourth-order Runge-Kutta algorithm with a typical timestep of 1 fm/c. Our numerical calculation is fully selfconsistent and conserves total energy to better than 0.1%.

We start with spherical distributions of nucleons in coordinate and momentum space, then introduce a temporary external potential in order to initiate a giant multipole oscillation of the nucleus. After the excitation, regular undamped motion of the collective multipole coordinate is observed for all cases. This contradicts the wall-formula prediction for a strongly damped octupole oscillation. A Fourier transform of collective coordinates shows a single peak at a dominant frequency and no ω^{-1} noise, indicating that no chaoticity is present in these coordinates. This result is surprising as the collective multipole coordinates are merely normalized sums of the single particle multipole coordinates, and the single particles can exhibit chaotic motion.

To investigate single particle motion, we test for sensitive dependence on initial conditions by finding the Lyapunov exponents. These exponents are a measure of the exponential divergence (or convergence) of initially nearby trajectories in phase space. A dynamical system has a positive Lyapunov exponent only if it is chaotic, and the lack of a positive Lyapunov exponent indicates the absence of chaos.

To calculate the Lyapunov exponents, we consider the motion of infinitesimal displacements from a trajectory in phase space, called tangent vectors. These displacements obey the linearized equations motion

$$\frac{d\mathbf{x}(t)}{dt} = J(t)\mathbf{x}(t)$$

where $\mathbf{x}(t)$ is the six-dimensional tangent vector and $J(t)$ is the Jacobian matrix of partial derivatives

evaluated along the trajectory in phase space. The ith Lyapunov exponent λ_i is defined as

$$\lambda_i = \lim_{t\to\infty} \frac{1}{t} \log_2 \left(\frac{\|\mathbf{x}_i(t)\|}{\|\mathbf{x}_i(0)\|} \right),$$

where $\|\mathbf{x}\|$ denotes the norm of $\mathbf{x}$ and the tangent vectors $\mathbf{x}_i(t), i = 1, \ldots, 6$, are orthogonal. The logarithm base two is used so that the units of the exponents are bits per time.

We follow the practical scheme of Wolf *et al.* [9] and numerically integrate the linearized equation for six orthogonal tangent vectors. Orthonormality of the vectors is maintained by applying the Gram - Schmidt algorithm between every timestep; the re-normalization of the vectors keeps them bounded and minimizes numerical error. The i^{th} tangent vector seeks the direction of most rapid growth in the subspace orthogonal to the $i-1$ previous tangent vectors.

We applied this method to twenty representative particles in the model and averaged their exponents together. The sum of the averaged exponents provides a check on accuracy; the sum should be zero as phase space volume is conserved in our system. In all cases the magnitude of the sum of the exponents was less than 10^{-7} bits c/fm. The results are given in table 1, which lists the largest Lyapunov exponent for each case. Note that the positive exponents are all significantly larger than 10^{-7}.

An interesting result comes from comparing the selfconsistent and the static cases for (Q_2, r^6). The former has chaos while the latter does not; we attribute the origin of this chaoticity to the exchange of energy between the single particles and the collective coordinate.

We show ordered collective motion resulting from underlying chaotic dynamics, something qualitatively new in our investigation. This agrees with the idea of the mean field (static or coherently oscillating) generated by averaging out random features of the motion of individual constituents. The smoothest component of single-particle dynamics survives after such averaging and gives rise to the self-consistent mean field. Therefore, chaos on a microscopic level does not necessarily lead to a catastrophic breakdown of the system on the macroscopic scale.

	selfconsistent		static	
	r^2	r^6	r^2	r^6
Q_2	0	$(2 \pm 1) \times 10^{-3}$	0	0
Q_3	$(4 \pm 1) \times 10^{-5}$	$(1.5 \pm 0.5) \times 10^{-3}$	$(8 \pm 2) \times 10^{-5}$	$(1 \pm 0.3) \times 10^{-3}$

Table 1: Values of the largest positive Lyapunov exponents obtained in the full selfconsistent calculations and in the calculations with static external multipole potentials. Units are bits c/fm.

a. On leave from Budker Institute of Nuclear Physics, 630090 Novosibirisk, Russia
b. Institut de Physique Nucléaire, Université de Grenoble, 53 avenue des Martyrs, 38026 Grenoble Cedex, France

References

1. D.L. Hill and J.A. Wheeler, Phys. Rev. 89(1953)1102.
2. J. Blocki et al., Nucl. Phys. A545(1992)511c; J. Blocki, J.-J. Shi, and W.J. Swiatecki, Nucl. Phys. A554(1993)387.
3. A. Bohr and B.A. Mottelson, *Nuclear Structure*, Volume II, p.350ff (W.A. Benjamin, Reading, Mass., 1975).
4. S. Stringari, Nucl. Phys. A325(1979)199; S. Stringari, Phys. Lett. 103B(1981)5.

5. H. Reinhardt and H. Schulz, Nucl. Phys. A391(1982)36.
6. H. Kohl, P. Schuck, and S. Stringari, Nucl. Phys. A459(1986)265.
7. G.P. Maddison and D.M. Brink, Nucl. Phys. A378(1982)566.
8. C.Y. Wong, Phys. Rev. C25(1982)1460.
9. A. Wolf et al., Physica 16D (1985) 285.

IN-MEDIUM EFFECTS ON THE NUCLEON-NUCLEON CROSS SECTION AND THE BUU TRANSPORT MODEL

W.Bauer and F.Daffin

It is known that nucleon-nucleon cross sections are modified in the presence of nuclear matter from their values in a vacuum. The total cross sections depend at least on the local baryon density, temperature, the momentum of the center of mass of the colliding nucleons relative to that of the local matter, and the energy of the colliding nucleons. The Boltzmann-Uehling-Uhlenbeck (BUU) transport model code used to simulate heavy-ion collisions has been modified to calculate these quantities. The modified cross sections have been calculated [1] and incorporated into the BUU collision term.

In order to incorporate the in-medium nucleon-nucleon cross secitons into the BUU program code, knowedge of the spacial distribution of the temperature, density and the momentum of the center of mass of the colliding particles relative to the local fermionic matter is needed.

At every time-step in the simulation, the momentum of the center of mass of each occupied in configuration space is calculated, stored and then subtracted from the momentum of the individual particles within that cell. This procedures eliminates effects of collective streaming and thus obtains the momentum of each cell due solely to random or thermal motion, and with it the thermal kinetic energy. From the mean kinetic energy and the mean density of a given cell, we obtain the local temperature by inverting the expressions

$$\mathrm{n} = \text{const.} \cdot \int dee^{1/2} \, (\exp((e-\mu)/T)+1)^{-1}$$

$$\mathrm{k} = \text{const.} \cdot \int dee^{3/2} \, (\exp((e-\mu)/T)+1)^{-1} \, .$$

Since the momentum of the center of mass of each occuped cell has been calculated, the momentum of the colliding nucleons relative to the matter within that cell is easily obtained. Finally, for each collision the in-medium nucleon-nucleon cross section is calculated via linear interpolation among its tabulated values. We are now studying the effects of the new cross sections on observable quantities of heavy-ion reactions.

References

1. T. Alm, G. Röpke, and M. Schmidt,"The In-Medium Nucleon-Nucleon Cross Section and BUU Simulations of Heavy-Ion Reactions," Rostock Preprint(1994).

CALCULATING COLLISION TERMS FOR PARTON BASED RHIC SIMULATIONS

J. Murray, G. Kortemeyer, S. Pratt, K. Haglin and W. Bauer

RHIC at Brookhaven will collide ^{197}Au+^{197}Au at a center of mass energy of 200 Gev/nucleon. At these energies partons are the relevant degree of freedom, and perturbative QCD can be used to calculate collision terms. The quarks and gluons are distributed within nucleons with momentum fractions goverened by parton distribution functions; the nucleons are in turn distributed within the Lorentz contracted nuclei, [1]. The interactions between partons that take place are strong interactions because QCD's coupling strength is larger than the electro-weak coupling. At present, only $2 \rightarrow 2$ scatterings and fusions are included in the simulation. The leading order processes that have been calculated are...

$$qq' \rightarrow qq', qq \rightarrow qq, q\bar{q} \rightarrow q\bar{q}, q\bar{q} \rightarrow q'\bar{q}'$$
$$qg \rightarrow qg, q\bar{q} \rightarrow gg, gg \rightarrow q\bar{q}, gg \rightarrow gg$$

Phenomenological screening or cut-off masses have been added into the propagators to avoid divergent total cross sections. However, the gluon-gluon scattering cross section includes a four point diagram which doesn't contain a propagator. This means that the divergence in this cross section must be handled differently from the other cross sections. Other methods of cutting off this cross section while maintaining the correct physics are being investigated. In addition, the gauge invariance of these cross sections with the screening masses will be studied. The expressions used in the simulation have been checked in the massless and massive limits [2],[3].

Once it is decided that a collision between partons will occur, the angular distribution of the outgoing partons, in the initial partons' center of momentum frame, is determined by a standard monte carlo that uses the perturbative cross section. Since gluons dominate the content of nucleons, the most frequent interactions will include a gluon in the initial state.

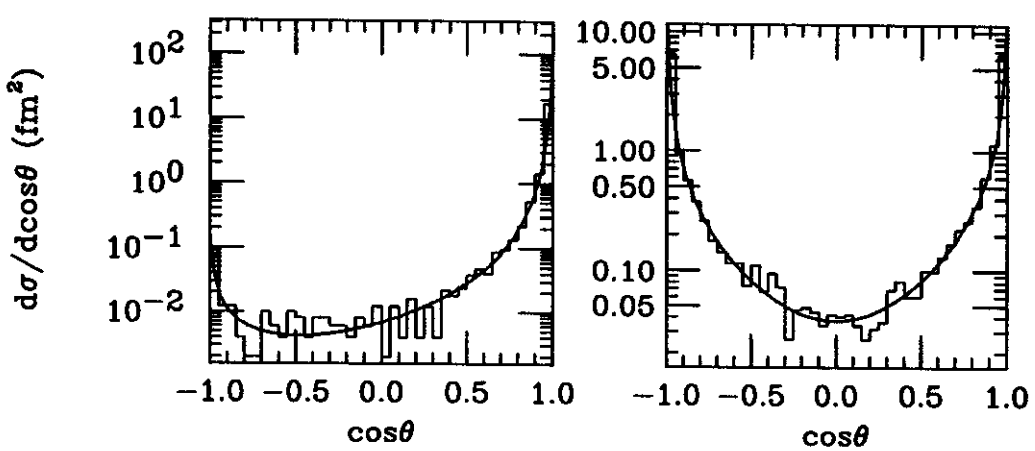

1. $qg \rightarrow qg$ monte carlo data and differential cross section at $\sqrt{s}$= 17 Gev. 2. $gg \rightarrow q\bar{q}$ monte carlo data and differential cross section at $\sqrt{s}$= 17 Gev.

In the future, $2 \rightarrow 1$ fusions and $1 \rightarrow 2$ decays will be included in the simulation. Splitting functions, which are related to the probability a parton will split into 2 other partons, are being calculated and studied, [4], [5]. Once these functions are understood, they can be implemented to govern the $1 \rightarrow 2$ decays in the model.

References

1. K. Geiger and B Müller, Nucl. Phys. B369 (1992), 600.
2. B.L. Combridge, J. Kripfganz, and J. Ranft, Phys. Lett. 70B, No. 2 (1977), 234.
3. E. Eichten, I. Hinchliffe, K. Lane, and C. Quigg, Rev. of Modern Phys. Vol. 56, No. 4 (1984), 579.
4. R.D. Field,Applications of Perturbative QCD, (Addison-Wesley Publishing Company, 1989).
5. G. Altarelli, G. Parisi, Nucl. Phys. B126 (1977), 298.

PARTON CASCADE FOR RHIC

G. Kortemeyer, J. Murray, S. Pratt, K. Haglin and W. Bauer

Introduction

The transport theory, so far being successfully applied to heavy ion collisions in the intermediate energy region, is being extended to high energy collisions. The main step in the extension of this microscopic model is using a parton based picture of the nuclei rather than a hadronic picture; consequently the interactions between the testparticles are to be described in the framework of QCD, leading to so-called parton cascades. The results of this simulation hopefully help to interpret first results from the BNL Relativistic Heavy Ion Collider (RHIC) at Brookhaven.

For a review of microscopic models being applied to heavy ion collisions in the intermediate energy region so far see [1]. For ultrarelavistic collisions transport theory has been applied to nucleon-nucleon collisions, see for example [2] using the Vlasov equation and [3] using parton cascades.

The microscopic simulation of recent heavy ion experiments like the proposed 200 GeV/nucleon ^{197}Au + ^{197}Au collider at Brookhaven however has only been done using parton cascades, see [4]. The same approach has been chosen in our simulation.

Implementation

Our code works in 3+1 dimensions using fully relativistic kinematics for the partons, where the quarks are consequently treated as massive particles. Both quarks and gluons can have off-shell masses. Interaction between the particles is mediated by QCD processes, no mean field or other means to guarantee confinement or the stability of the nuclei are implemented so far. No medium modifications to the elementary cross sections are taken into account so far.

Open Questions

Initialization

The initialization of the partons is done according to the parton distribution functions $f_\alpha(x, Q^2)$, $\alpha = g, u, \bar{u}, d, \bar{d} \ldots$. Three questions arise immediately: What is the spatial distribution of the partons? As the parton distribution functions diverge with small x, what is the minimum x to be chosen? Finally, how is the parameter Q^2 to be chosen?

For the spatial distribution at the moment the partons are randomly placed within a highly Lorentz contracted sphere of given nucleonic radius. Geiger [3] is using the "wee parton" model having the softer partons being smeared out even outside the Lorentz contracted radius of the nucleons, resulting in a minimum width of the nucleon pancake of about 1 fm in any frame of reference.

The x cutoff will remain a parameter of the model, it has to be chosen such that the simulation reproduces nucleon-nucleon scattering data, however not taking into account in-matter effects.

In other approaches Q^2 so far has been chosen corresponding to c.m.-energy available for the collisions between partons from the colliding nuclei. It was then iteratively adjusted to the c.m.-energies really found in different runs of the program.

However, once a parton has scattered with a parton from the other nucleus it can scatter with fellow partons from the same nucleus at much lower c.m.-energies.

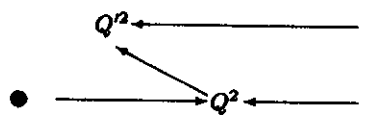

As a result, there are two classes of interactions: The high energy interactions between partons from different nuclei, which are viewed with a high parton resolution, and lower energy collisions between partons from the same nucleus, which are viewed with a much smaller parton resolution.

How these two classes of parton resolutions can be accomplished with one initial parton distribution has not yet been studied.

The effects of different models for the initial parton distribution will be examined.

Soft Processes

For the soft processes between partons from the same nucleus mentioned above, a problem with the elastic gluon-gluon cross section arises: In the 4-point component of the cross section no screening mass can be introduced, resulting in the divergence of the cross section for the c.m.-energy $\sqrt{s} \to 0$. Different methods of dealing with the soft processes in the framework of our simulation will be subject of studies.

Hadronisation

No hadronisation scheme has been implemented so far. A simple scheme suggested by Geiger based only on distances both in configuration and momentum space might be a start. Other possibilities under consideration are "coalescence," "self-similar tree structure," or even "fractal structure." The study of different hadronization schemes will be a large part of our research.

Superluminar Signals

An inherent problem of transport codes is that subsequent non-retarded interactions lead to signal transport with velocities faster than the speed of light. This problem will especially occur in ultrarelativistic parton cascades since the timesteps have to be chosen smaller and low-energy interactions are not surpressed so that the damping of outgoing signals is very low.

First Results

The code so far runs only with realistic QCD interactions for two incoming and two outgoing particles. Particle production and decay processes have not yet been implemented. First studies on superluminous signals were performed, see separate report.

Outlook

The calculation of photon and lepton pair production will give the opportunity to calibrate the model with experiment. The model dependence on the energy density will be studied, insights on the approach to thermalization and/or equilibration will hopefully be gained. The investigation of different hadronization schemes will hopefully help to gain more understanding of this critical part of any parton cascade model.

References

1. G. F. Bertsch and S. Das Gupta, Phys. Rep. 160, No. 4 (1988), 189
2. U. Kalmbach, T. Vetter, T. S. Biró and U. Mosel, Nucl. Phys. A563 (1993), 584
3. K. Geiger and B. Müller, Nucl. Phys. A544 (1992), 467c
4. K. Geiger, *Proc. XXVI Int. Conf. on High Energy Physics, Dallas*, Vol. 1, 977

CAUSALITY VIOLATIONS IN CASCADE CALCULATIONS

G. Kortemeyer, J. Murray, S. Pratt, K. Haglin and W. Bauer

Introduction

Parton cascade codes work by propagation of the testparticle configuration in discrete timesteps of a fixed length Δt_{step}. An inherent problem of transport codes is that subsequent non-retarded interactions lead to information transport with velocities faster than the speed of light. The velocity of such signals can approach $\sqrt{\frac{\sigma}{\pi}}/\Delta t_{\text{step}}$, where σ is the cross section of the interaction. This problem is especially serious in ultrarelativistic parton cascades since the timesteps have to be chosen smaller and low-energy interactions are not surpressed so that the damping of outgoing signals is very low.

Signal Propagation

When talking about information transport we are mainly concerned about information being propagated in the transverse direction. An example for such transport is given in the following figure:

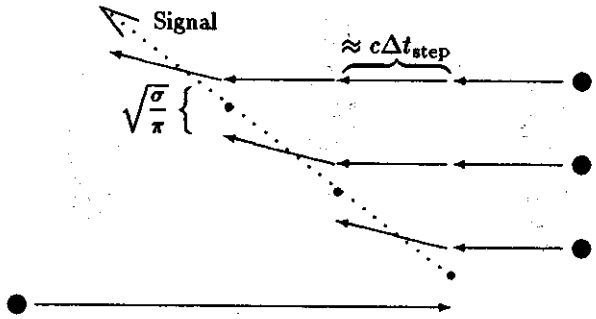

In the figure one particle coming from the left scatters with another particle coming from the right. As part of the model the scattered particles can not scatter again in this timestep. However, one timestep later that scattered particle from the right scatters with another particle coming from the right. As a result information from the first scattering, for example about momenta and particle types, has travelled to the second one.

This kind of information transport can continue over several scattering events. As the signal can travel over the diameter of the cross section σ in just one timestep and then continue it's propagation over more than one timestep the signal velocity can reach the velocity $\sqrt{\frac{\sigma}{\pi}}/\Delta t_{\text{step}}$ over several timesteps. This is a general problem of all transport codes, however, as the gluon-gluon cross section reaches rather high sizes instead of vanishing for low c.m.-energies, subsequent scattering events are not damped, and also as gluon densities are very high, the probability for scattering in two immediately subsequent timesteps is very high. It is to be pointed out that the "closest point" approach for interactions times has no effect on this violation of causality in the transverse direction.

Results

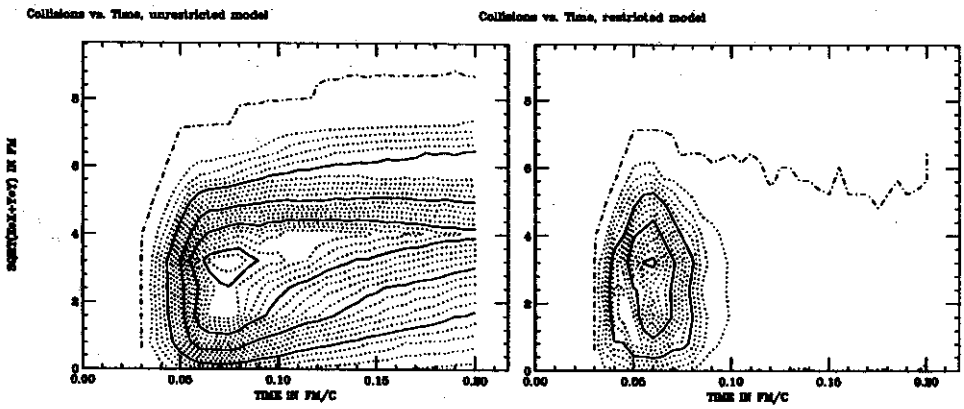

The code was run for the collision of two Au-nuclei with 3 fm impact parameter. So far only processes with two partons in the incoming and outgoing state were implemented, we had approximately 17,000 partons per testrun with 5 parallel testruns for better statistics. The above figure shows the distance of collisions from the $x = y = 0$ axis in fm versus the time since the simulation was started. The figure on the left is

the result of a calculation with no restrictions on signal propagation, the figure on the right results from a calculation where signal transport with velocities faster than light was explicitly forbidden. Namely, interactions with $|\vec{r}_j - \vec{r}_i|/(t_j - t_i) \geq c$ were considered impossible, where x_j refers to the coordinates of the midpoint of the collision in question, and x_i to the last collision of one of the partons involved.

It turns out that indeed in the restricted model the signal propagation inside the nuclei is damped after the initial collisions with partons from the other nucleus, while in the unrestricted model the shock wave keeps expanding. At low energies the gluon-gluon cross section was cut off at 5 fm^2, the gluon density is high enough to make the gluons scatter in every timestep. Analyzing the signal velocities, one can indeed find signals travelling with the above calculated maximum velocity.

With the timestep length of 0.005 fm/c and a gluon-gluon cross section of 0.5 fm^2 this maximum velocity is approximately 80c. Looking at a projection of the parton densities from above one can see that in the unrestricted model the center region is expanding faster than in the restricted model.The picture shows the configuration of 0.17 fm/c after the first collisions.

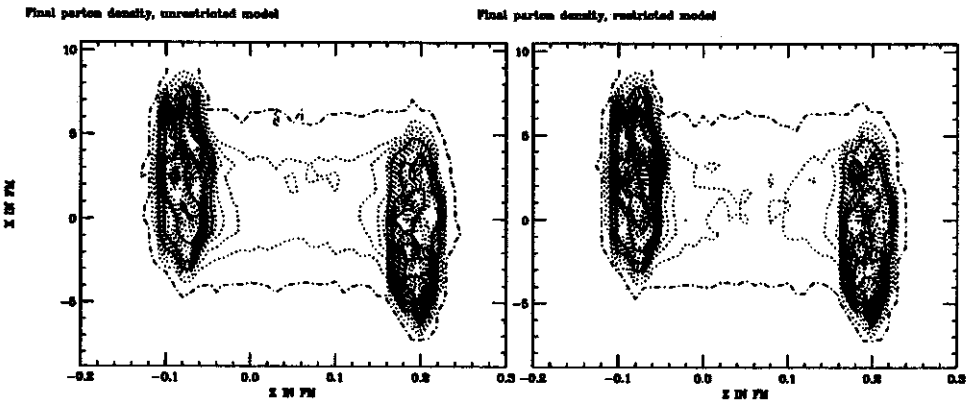

However, the differences can more clearly be seen in the rapidity distributions. The partons from the two nuclei come in with about 6 units of rapidity, right after the first collisions many partons lose several units of rapidity, resulting in gaps in the rapidity distribution between the scattered and the unscattered partons. As the collision rate is higher in the unrestricted model those gaps wash out quite soon, which they don't in the restricted model. The rapidity region around zero however looks the same in both models:

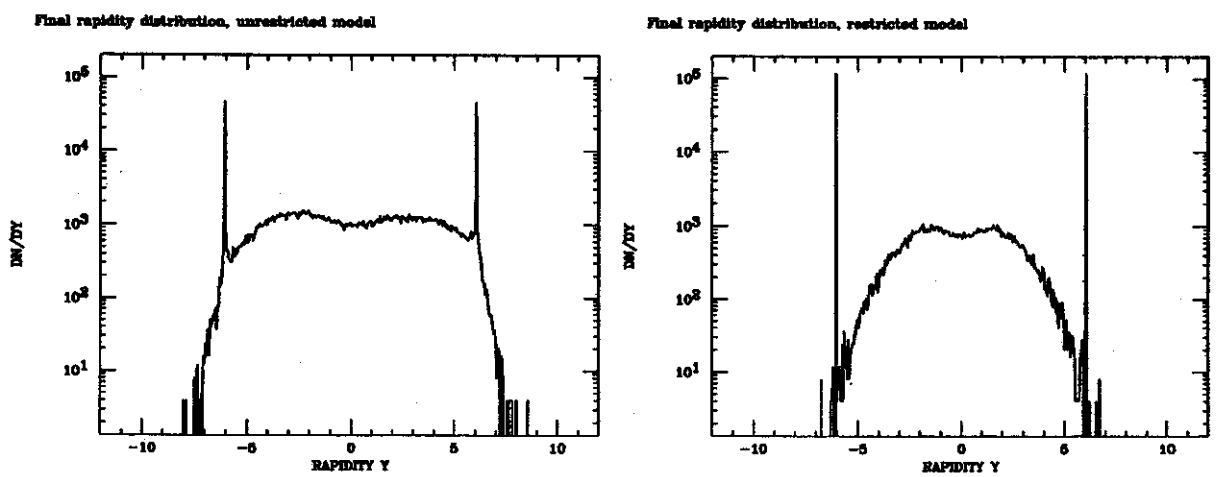

Outlook : We are studying further the effects of superluminar signals in the context of various scattering prescriptions.

DILEPTON PRODUCTION IN PROTON+NUCLEON COLLISIONS

Kevin Haglin

It has been argued over and over that the dipole approximation of proton-nucleon bremsstrahlung is a good one, even for Bevalac energies. This means that one would argue that np bremsstrahlung is a much stronger contributor to e^+e^- production than pp. If this were true one would expect that the pd/pp ratio is not too small. The np component allowed by the target deuteron would clearly dominate—pushing this ratio to something large. Yet, the experimentally observed ratios are 10 at 1.0 GeV with monotonic decrease to nearly 2 at 4.9 GeV[1,2]. Resolution is suggested after careful re-examination of simple nucleon-nucleon bremsstrahlung calculations for these energies as well as a serious examination of bremsstrahlung beyond two-to-two hadronic reactions. We investigate the effects of pions in the final state since the energies of interest are clearly above pion production thresholds. We find their effect to be most important[3,4].

We start with a completely general hadronic reaction $a + b \to 1 + 2 + \ldots + n$. In the soft-photon approximation, the scattering amplitude for radiation off the external lines diverges since the half off shell hadron approaches its mass shell. All the rest, dubbed internal radiation, stay finite. To a good approximation, they can be neglected. Then, the matrix element for soft-photon production simplifies to the purely hadronic counterpart times a multiplicative function describing the complicated electrodynamics of the reaction[5]. Partially correcting for phase space and insisting on energy conservation at the photon-dilepton vertices, the differential cross section for pure hadronic scattering (elastic or inelastic) while at the same time producing a virtual photon (electron-positron pair) of invariant mass M and energy q_0 is

$$\frac{d\sigma^{e^+e^-}}{dM} = \frac{\alpha^2}{4\pi^4}\frac{1}{M}\int \delta(q^2 - M^2)\delta^4(q - (p_+ + p_-))\, d^4q \left(\frac{\widehat{\sigma}(s)}{q_0^2}\right) \frac{d^3p_+ d^3p_-}{E_+E_-}\frac{R_n(s')}{R_n(s)}, \tag{1}$$

where R_n is n-body phase space[6], $s' = s + M^2 - 2\sqrt{s}\,q_0$, and

$$\widehat{\sigma}(s) \equiv \int \prod_{i=1}^{n} d^3p_i \left[\frac{d^{3n}\sigma}{\prod_{i=1}^{n} d^3p_i}\right] \left(q_0^2\,|\epsilon \cdot J|^2\right). \tag{2}$$

The bracketed expression in Eq. (2) is the purely hadronic cross section and $q_0^2|\epsilon \cdot J|^2$ is the dimensionless electromagnetic *weighting* representing a coherent sum of all radiating external lines in the diagrams[8].

Hadronic cross sections are input for the soft-photon calculations we are discussing. Precise forms we take for differential np and pp cross sections have been published elsewhere[4], so we do not reproduce them here. But we stress the importance of choosing parametrizations that account for observed angular dependences of the cross sections. Upon integrating Eq. (1) with the DLS acceptance version 2.0 included, we arrive at a cross section.

In Fig. 1a we show the one-pion channels' contributions in pp scattering as compared with simple bremsstrahlung and DLS data[7]. Though not shown here, np simple bremsstrahlung is lower than pp bremsstrahlung by a factor ~ 1.5. The double pion channels are intermediate between these and simple bremsstrahlung, but fall faster with increasing mass due to phase space. Finally, the three pion channels

contribute roughly the same as the two-pion channels at very low mass, but phase space cuts them off even faster. When all the channels are added together we arrive at the total *pp* bremsstrahlung shown in Fig. 1b as open squares. One concludes that bremsstrahlung is indeed the largest source of dielectrons and that it comes from many-body bremsstrahlung. Also included in Fig. 1b are results from η Dalitz, radiative Δ decay and an estimate of $\pi^+\pi^-$ annihilation[9]. Details can be found in Ref. [4].

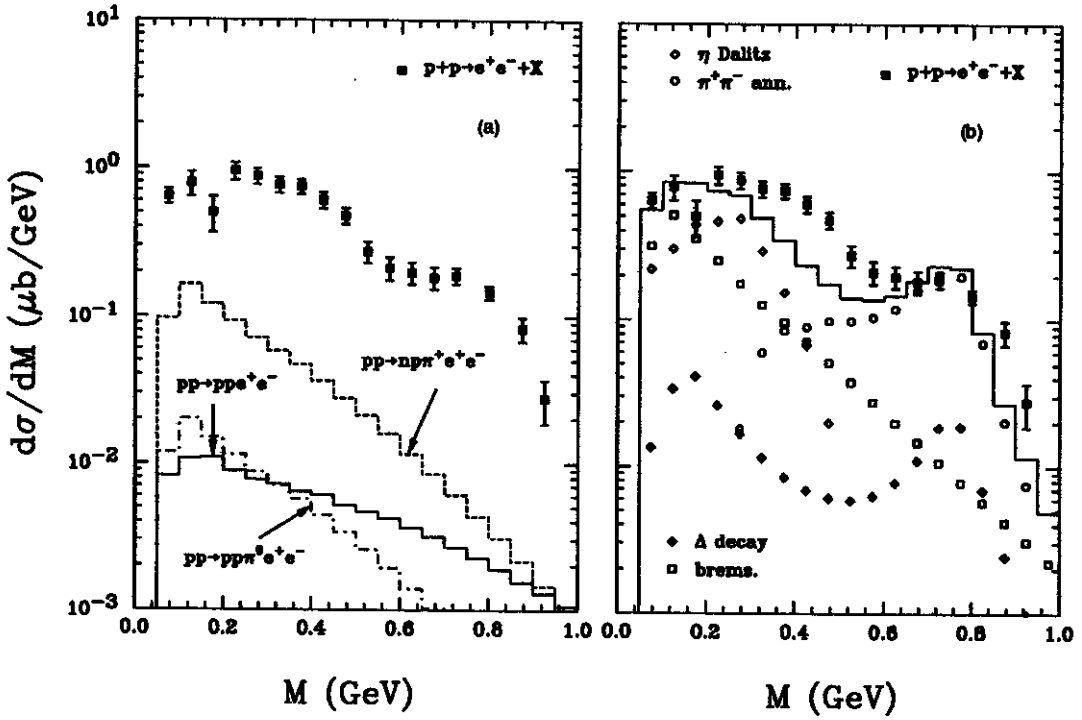

Fig. 1: Invariant mass distribution from single pion channels (a) and from several different sources (b) as compared with inclusive *pp* results at 4.9 GeV from the Bevalac. Solid histogram in (b) is the sum of all four sources.

Proton-proton bremsstrahlung is as strong or stronger than proton-neutron at Bevalac energies. Hadronically inelastic channels, i.e. single and double pion channels, are more important to low-mass dielectron production than simple bremsstrahlung and even η Dalitz decays. Observed *pd*/*pp* dielectron production ratios can be understood by including simple and many-body bremsstrahlung, Dalitz and radiative decays and two-pion annihilation. A more detailed study of the ratios properly incorporating the target deuteron and also isospin differences in η production (and therefore Dalitz decays) must be done.

References

1. H. Z. Huang, *et al.*, Phys. Lett. B 297, 233 (1992).
2. W. K. Wilson, *et al.* Phys. Lett. B 316 (1993).
3. K. Haglin, LBL Special Report of the 9th High-Energy Heavy Ion Study, Oct. 1993.
4. K. Haglin and C. Gale, Phys. Rev. C 49, 401 (1994).
5. L. Heller, *Soft Lepton Pair and Photon Production*, edited by J. A. Thompson (Nova Science, 1992), p. 1.
6. E. Byckling and K. Kajantie, *Particle Kinematics* (John Wiley & Sons, 1973).
7. H. Z. Huang, *et al.*, Phys. Rev. C 49, 314 (1994).
8. K. Haglin, V. Emel'yanov and C. Gale, Phys. Rev. D 47, 973 (1993).
9. J. Kapusta and P. Lichard, Phys. Rev. C 40, R1574 (1989).

ON THE MEAN FREE PATHS OF PIONS AND KAONS IN HOT HADRONIC MATTER

Kevin Haglin and Scott Pratt

By measuring outgoing hadrons in a heavy-ion collision one can reconstruct a reaction's breakup stage. The momenta of outgoing particles can be measured directly and a space-time picture of the last collisions may be constructed using the techniques of two-particle interferometry[1]. Space-time information is especially useful. For instance, if the time a reaction takes to proceed is much longer than 10 fm/c, it would signal a reduction in pressure, inferring a first-order phase transition[2].

We study mean free paths of pions and kaons at temperatures and densities characteristic of hadronic matter from the breakup stage of a relativistic heavy-ion collision at CERN[3]. We find that in this environment mean free paths are remarkably similar and conclude that information from kaon interferometry describes the dissolution of the entire system, as kaons should escape at the same time as pions which comprise the bulk of the matter. In the context of a thermodynamic model we estimate mean free paths of a meson of type a given its momentum. Assuming the meson interacts with an assortment of hadrons of type b whose density is given according to a relativistic Boltzmann distribution and assuming we know the cross sections σ_{ab}, the mean free path is:

$$\lambda_a(p_a) = \frac{p_a}{E_a} \frac{1}{R_a^{net}(p_a)}. \tag{1}$$

Here p_a and E_a represent the meson's momentum and energy while R_a is the collision rate. The net collision rate includes contributions from all different species.

$$R_a^{net}(p_a) = \sum_b R_{ab}(p_a) \tag{2}$$

$$R_{ab}(p_a) = \int ds \frac{d^3p_b}{(2\pi)^3} f(p_b) \sigma_{ab}(s) v_{rel} \delta\left(s - (p_a + p_b)^2\right)$$

where

$$v_{rel} = \frac{\sqrt{(p_a \cdot p_b)^2 - m_a^2 m_b^2}}{E_a E_b}, \qquad f(p_b) = (2s_b + 1) e^{-(E_b - \mu)/T}.$$

Only baryons are given a chemical potential which is chosen to result in a free π^+ to proton ratio of 10. Species included in the calculation are π, K, ρ, η, ω and K^*.

Cross-sections are dominated by contributions of resonances. For pions the largest contributor to the collision rate is the resonant reaction through the ρ while for kaons the most common collision is with pions through the K^* resonance. Heavier resonances are also included.

The average mean free path is obtained by

$$\bar{\lambda} = \frac{\int d^3p f(p) \lambda(p)}{\int d^3p f(p)}. \tag{3}$$

Results are shown in Fig. 1.

The reaction should end when the mean free path is near the size of the system. From interferometry the size of the dissolving system appears similar to the size of a lead nucleus which has a radius of seven fm. A mean free path of seven fermi corresponds to a temperature of approximately 110 MeV. One must be cautious of such conclusions both because of the lack of geometric detail involved in the inference and the questionable assumption of zero chemical potential. Rapid expansion can outrun a system's ability to stay in chemical equilibrium, resulting in large chemical potentials[4,5,6], higher densities and therefore shorter mean free paths. This would allow the system to stay together longer, resulting in lower breakup temperatures.

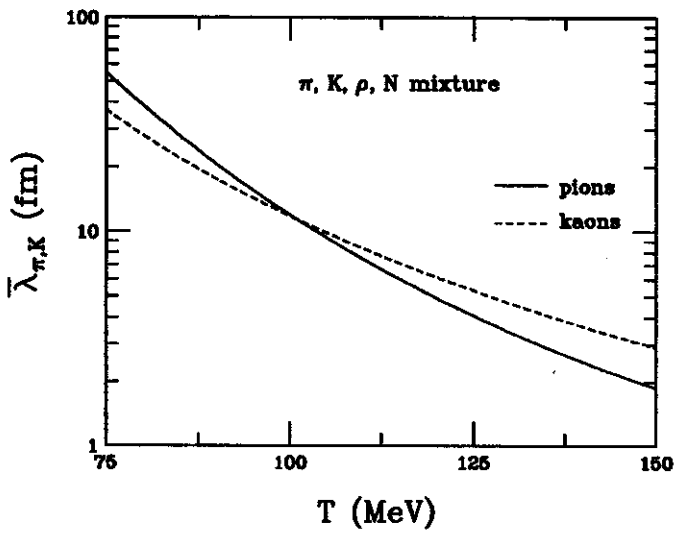

Fig. 1: Average mean free paths of pions (solid curve) and kaons (dashed curve) as they depend on the temperature.

Notice from Fig. 1 that the mean free paths of kaons and pions are so similar. This means that kaons can be used to view the final stage of the collision without the qualification that they have escaped prematurely. This does not mean that correlation functions from kaons and pions should have the same apparent source sizes, and indeed at CERN preliminary measurements point to smaller sizes for kaons than pions[7]. Even if one can account for pions from long-lived resonances, kaon sources can appear smaller due to collective expansion. A heavier particle with a given velocity is more confined to the region with the same collective velocity[8,2]. Given that pions and kaons have such similar escape probabilities, one can then compare and interpret correlation results from kaons and pions. This clarifies the meaning of both measurements.

References

1. S. Pratt *et al.*, Nucl. Phys. A566 (1994) 103c.
2. S. Pratt, Phys. Rev. D 33 (1986) 1314.
3. K. Haglin and S. Pratt, Phys. Lett. B, in press.
4. S. Gavin and P. V. Ruuskanen, Phys. Lett. B262 (1991) 326.
5. G. M. Welke and G. F. Bertsch, Phys. Rev. C 45 (1992) 1403.
6. P. Gerber, H. Leutwyler and J. L. Goity, Phys. Lett. B243 (1990) 18.
7. T. J. Humanic (NA44 Collaboration), Nucl. Phys. A566 (1994) 115c.
8. S. Pratt, Phys. Rev. Lett. 53 (1984) 1219.

PROPERTIES OF THE PHI MESON AT FINITE TEMPERATURE

Kevin Haglin and Charles Gale[a]

We calculate the ϕ-meson propagator at finite temperature at one-loop order[1]. The real and imaginary parts are studied separately in full kinematic ranges. From this activity we investigate how temperature affects such things as decay widths and dispersion relations. We also estimate the thermal rate of lepton pair radiation in a hadron gas proceeding through $K^+K^- \to \phi \to \ell^+\ell^-$ and $\pi\rho \to \phi \to \ell^+\ell^-$.

Vector mesons interact in a renormalizable fashion with a conserved current. The full Lagrangian for K-ϕ dynamics is

$$\mathcal{L} = \frac{1}{2}|D_\mu K|^2 - \frac{1}{2}m_K^2|K|^2 - \frac{1}{4}\phi_{\mu\nu}\phi^{\mu\nu} + \frac{1}{2}m_\phi^2\phi_\mu\phi^\mu, \tag{1}$$

where K is the complex charged kaon field, $\phi_{\mu\nu} = \partial_\mu\phi_\nu - \partial_\nu\phi_\mu$ is the ϕ field strength tensor, and $D_\mu = \partial_\mu - ig_{\phi KK}\phi_\mu$ is the covariant derivative. This gives rise to two diagrams which contribute to the self-energy at the one-loop level shown in Figs. 1a and b. We go further by including a ϕ-ρ-π interaction given by the Lagrangian[2]

$$\mathcal{L}_{\rm int} = g_{\phi\rho\pi}\epsilon_{\mu\nu\alpha\beta}\partial^\mu\phi^\nu\partial^\alpha\rho^\beta \cdot \pi, \tag{2}$$

where the complex charged rho and pion fields appears as ρ^β and π. This term gives the diagram shown in Fig. 1c.

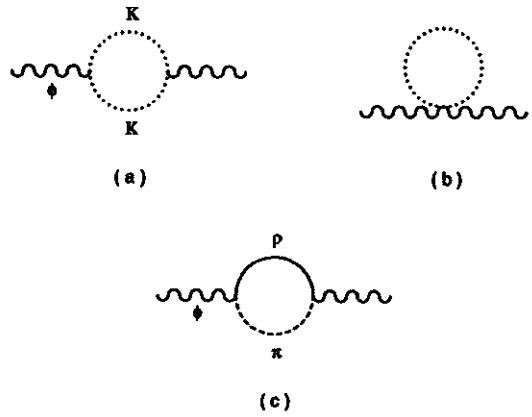

Fig. 1: One loop contributions to the self-energy: (a) and (b) are bubble and tadpole kaon contributions while (c) is a $\pi\rho$ contribution.

The self-energy is decomposed into scalar functions times the standard longitudinal and transverse projection tensors as[3]

$$\Pi^{\mu\nu}(k) = F(k)P_{\rm L}^{\mu\nu} + G(k)P_{\rm T}^{\mu\nu}. \tag{3}$$

By studying the functions F and G at nonzero temperature we learn how physically meaningful quantities such as decay widths, effective masses, and so on, behave. A notion more general than effective mass is dispersion. In Fig. 2 the dispersion relation for longitudinally polarized phi mesons are presented at three values of temperature. The effect of temperature is small but the direction of it is quite clear: We see an increase in the effective mass with temperature.

We have learned that within this type of modelling for the relevant hadronic degrees of freedom and their (strong) interaction, the effective mass of the ϕ-meson is nearly temperature independent below

~ 50 MeV. Above this, it shows slight increase: It rises by 0.42, 1.55, and 4.59 MeV at temperatures 100, 150 and 200 MeV, respectively.

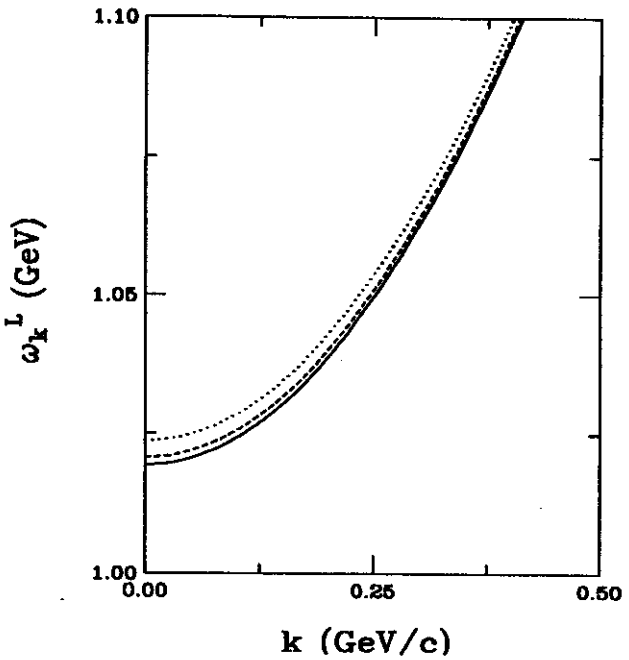

Fig. 2: Dispersion relation for longitudinally polarized ϕ-mesons at zero (solid curve) and finite temperature (dashed curve T=150 MeV and dotted curve T= 200 MeV).

This rise is mostly due to the kaon contributions, although the effect of the $\pi\rho$ channel is to move the mass in the same direction. The partial decay width into the $\pi\rho$ channel is the most affected by temperature. Since it is smaller than the kaon channel to begin with, the net result for the width's modification is also modest. At 150 MeV temperature, the width increases by 11% and at 200 MeV temperature it increases by 23% as compared to its vacuum value. The thermal rate of dielectron production near the ϕ mass was shown to be altered accordingly. Polarization effects are insignificantly small.

a. Physics Department, McGill University, Montréal, QC, H3A 2T8, Canada.

References

1. K. Haglin and Charles Gale, Nucl. Phys. B, in press.
2. U.-G. Meißner, Phys. Rep. 161, 215 (1988).
3. $P_T^{00} = P_T^{i0} = P_T^{0i} = 0$, $P_T^{ij} = \delta^{ij} - k^i k^j/k^2$, and $P_L^{\mu\nu} = k^\mu k^\nu - g^{\mu\nu} - P_T^{\mu\nu}$.

HANBURY-BROWN–TWISS ANALYSIS IN A SOLVABLE MODEL

G.F. Bertsch[a,b], P. Danielewicz, and M. Herrmann[a]

The analysis of meson correlations by Hanbury-Brown–Twiss (HBT) interferometry is tested [1] with a simple model of meson production by resonance decay.

The basic observables within the HBT analysis are the one- and two-particle differential cross sections, $d\sigma^{(1)}/d^3q$ and $d\sigma^{(2)}/d^3q_1 d^3q_2$, in some class of events. With the cross section for those events denoted as σ_0, the doubles-to-singles correlation function is defined as

$$C^{\mathrm{d/s}}(q_{\mathrm{av}}, q_{\mathrm{rel}}) = \sigma_0 \frac{d\sigma^{(2)}}{d^3q_1 d^3q_2} \Big/ \frac{d\sigma^{(1)}}{d^3q_1}\frac{d\sigma^{(1)}}{d^3q_2}\,. \tag{1}$$

To facilate later on the interpretation of the correlation function, we chose the arguments to be the average and relative momentum, $q_{\mathrm{av}} \equiv (q_1+q_2)/2$ and $q_{\mathrm{rel}} \equiv q_1 - q_2$, respectively. We further find it also useful to analyze correlations in our model by dividing the two-particle cross section by the unsymmetrized cross section, such as in the case of unlike mesons,

$$C^{\mathrm{l/u}}(q_{\mathrm{av}}, q_{\mathrm{rel}}) = \frac{d\sigma^{(2)}}{d^3q_1 d^3q_2} \Big/ \frac{d\sigma_u^{(2)}}{d^3q_1 d^3q_2}\,. \tag{2}$$

Within the HBT analysis, under assumptions that, in particular, involve the factorization of unsymmetrized two-particle phase-space distribution,

$$g^{(2)}(x_1, q_1; x_2, q_1) = g^{(1)}(x_1, q_1)\, g^{(1)}(x_2, q_2)\,. \tag{3}$$

either correlation function may be related to the one-particle distribution $g^{(1)}$ [2],

$$C(q_{\mathrm{av}}, q_{\mathrm{rel}}) = 1 + \frac{\int d^4x_1 d^4x_2\, g^{(1)}(x_1, q_{\mathrm{av}}) g^{(1)}(x_2, q_{\mathrm{av}}) \cos q_{\mathrm{rel}}(x_1 - x_2)}{\int d^4x_1 g^{(1)}(x_1, q_1) \int d^4x_2 g^{(1)}(x_2, q_2)}. \tag{4}$$

Our model is based on a picture of a small source that emits heavy resonances that propagate and decay by emitting a meson, see Feynman graphs in Fig. 1. Up to a constant factor the differential cross section for pion emission is given by

$$\begin{aligned}\frac{d\sigma^{(2)}}{d^3q_1 d^3q_2} &= \frac{1}{2}\frac{1}{\omega(q_1)\omega(q_2)} \int dk_1\, dk_2\, \Omega^{(N)}(E - E_1 - E_2, P - P_1 - P_2) \Big| G_r(E_1, P_1) G_r(E_2, P_2) \\ &\quad + G_r(E_1 + \omega(q_2) - \omega(q_1), P_1 + q_2 - q_1)\, G_r(E_2 + \omega(q_1) - \omega(q_2), P_2 + q_1 - q_2) \Big|^2, \end{aligned} \tag{5}$$

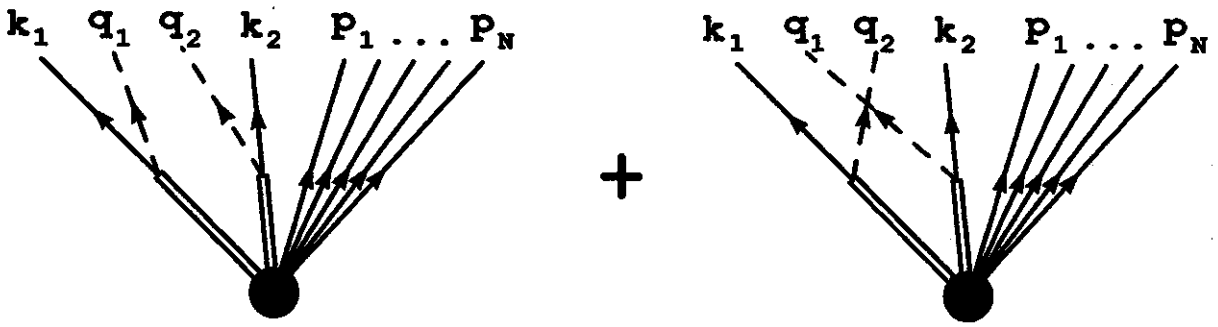

Figure 1: Graphical representation of the symmetrized amplitude for the production of two mesons in our model.

where $\Omega^{(N)}$ is N-particle phase-space volume, $E_i \equiv \epsilon_f(k_i) + \omega(q_i)$. The resonace propagator G_r is

$$G_r(E,\boldsymbol{P}) \equiv \frac{1}{E - \epsilon_r(\boldsymbol{P}) - m_{\rm diff} + i\Gamma_r/2} \tag{6}$$

where $\epsilon_r(\boldsymbol{P}) \equiv \boldsymbol{P}^2/2m_r$, and $m_{\rm diff} \equiv m_r - m_f$ is the difference between resonance mass and the mass of an unobserved particle in the final state. We choose $m_\pi = 139$ MeV, $m_f = 939$ MeV, $m_r = 1232$ MeV, $\Gamma_r \equiv \Gamma_\Delta = 115$ MeV, and work for simplicity in one dimension.

Figure 2 shows typical results for $C^{\rm d/s}$ calculated with Eq. (5). The deviations from the thermal $N \to \infty$ limit for finite N are associated with recoil effects that lead to the violation of Eq. (3). Following (4) the correlation function should start at 2 at zero $q_{\rm rel}$ and fall monotonically to 1 at large $q_{\rm rel}$. It is quite apparent in Fig. 2 that even in thermal limit the correlation function does not follow such behavior. This can be followed to the effect of symmetrization on one-particle distribution, cf. Eq. (3). The effect is large, of the order of 25% in our model, when the inverse of the source size is comparable to size of meson momentum space. Effects of comparable magnitude were found in the past in the analyses of data [3,4].

Problems with the effects of symmetrization in normalizing the correlation function are absent in (2). In data analysis in the past, the removal of the effects of symmetrization in normalizing the correlation function has been attempted in Refs. [5,3]; see further [1]. The correlation function from (2) in thermal limit is shown in Fig. 3. It behaves as expected on the basis of Eq. (4).

Following (4) the inverse of a width of the correlation function in relative momentum gives a size of the emission region. Classically, the resonances decaying at a rate $1/\Gamma_r$ should give an r.m.s. size independent of the temperature, $< x^2 >_{\rm cl}^{1/2} = \sqrt{2} v_r/\Gamma_r$. However, it is apparent in Fig. 3 that the size of the emission region within our model depends on the temperature; see further Fig. 4. Primarily, at temperatures of the order pion mass most resonances are emitted with masses m that are below m_r. If $|m - m_r| > \Gamma_r/2$, then the resonance may be considered a virtual particle that lives a time given by the inverse of particle virtuality $1/|m - m_r|$ rather than $1/\Gamma_r$. Explicitly we find within our model that the

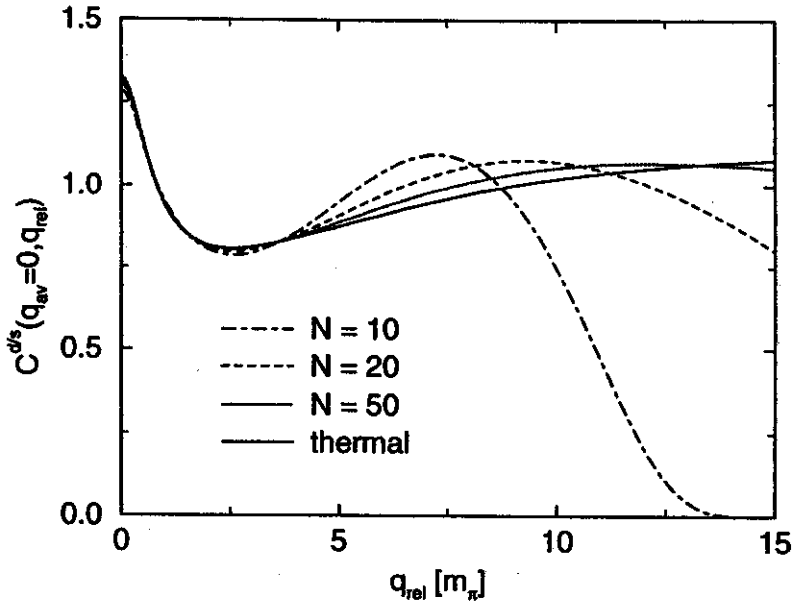

Figure 2: Correlation function $C^{\mathrm{d/s}}$ for different numbers of particles and in the thermal limit. The energy is $E = 1.5Nm_\pi$ which corresponds in the thermal limit to a temperature of $T = 3\,m_\pi$. The average momentum of the meson pair is zero for all cases.

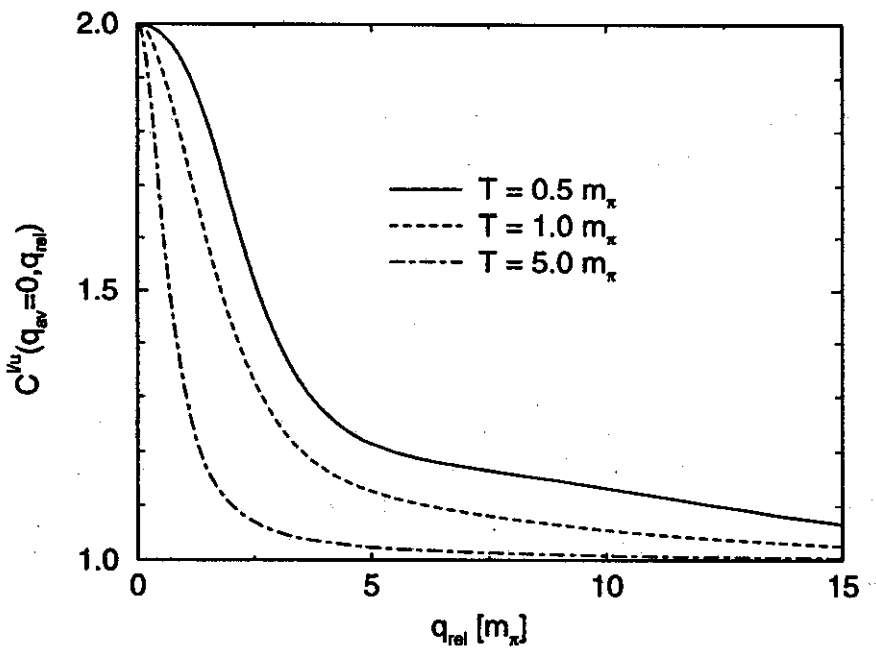

Figure 3: The correlation function $C^{\mathrm{l/u}}$ for different temperatures $T = 0.5m_\pi$ (full line), $1.0m_\pi$ (dashed line), and $5.0m_\pi$ (dot-dashed line). The width of the resonance is $\Gamma_r = \Gamma_\Delta$.

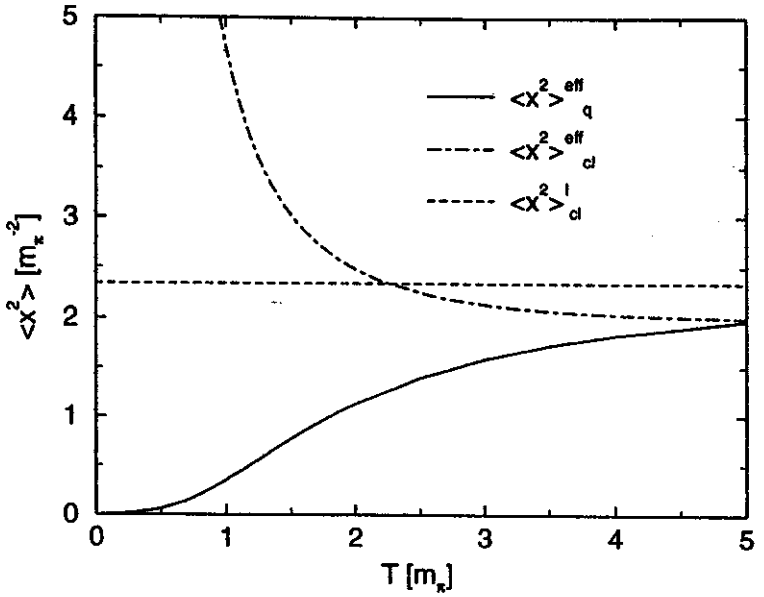

Figure 4: The mean square source size as a function of the temperature in various treatments. The horizontal dashed line is the classical size. The dot-dashed curve includes corrections to the size of the classical source. The solid line gives the result from the quantum mechanical calculation. The width is $\Gamma_r = \Gamma_\Delta$.

mean square radius deduced from the correlation is

$$< x^2 >^{\rm eff} = \left\langle\left\langle \frac{v_r^2}{(\Delta E)^2 + (\Gamma_r/2)^2} \right\rangle\right\rangle, \tag{7}$$

which is consistent with the above consideration. We used $\Delta E = \epsilon_r(k + q_{\rm av}) + m_{\rm diff} - \epsilon_f(k) - \omega(q_{\rm av})$ in (7) and the thermal average $\langle\langle f \rangle\rangle$ weighted by the resonance distribution is defined as

$$\langle\langle\, f \,\rangle\rangle \equiv \frac{\int dk\; {\rm e}^{-\epsilon_f(k)/T} f \left((\Delta E)^2 + (\Gamma_r/2)^2\right)^{-1}}{\int dk\; {\rm e}^{-\epsilon_f(k)/T} \left((\Delta E)^2 + (\Gamma_r/2)^2\right)^{-1}}. \tag{8}$$

To summarize, we find that for small number of particles ($\lesssim$15 in 3 dimensions) recoil effects may play a role in the correlation function. When normalizing correlation function using single-particle cross sections, the effect of correlations onto the latter need to be eliminated within the analysis. Strong quantum effects in the source size indicate an importance of the off-shell propagation for resonances at the temperatures of interest in nuclear collisions.

a. Institute for Nuclear Theory, HN-12, University of Washington, Seattle, WA 98195.
b. Physics Department, FM-15, University of Washington, Seattle, WA 98195.

References

1. G. F. Bertsch, P. Danielewicz and M. Herrmann, Phys. Rev. C 49 (1994) 442.

2. S. Pratt, Phys. Rev. Lett. 53 (1984) 1219.
3. H. Bøggild *et al.*, Phys. Lett. B302 (1993) 510.
4. K. Kadija and P. Seyboth, Phys. Lett. B287 (1992) 363.
5. W. Zajc *et al.*, Phys. Rev. C 29 (1984) 2173.